Vol. 256: 13–27, 2003 | MARINE ECOLOGY PROGRESS SERIES
Mar Ecol Prog Ser | Published July 17

Phytoplankton production in the North Water Polynya: size-fractions and carbon fluxes, April to July 1998

Zhi-Ping Mei[1,6,*], Louis Legendre[1,2], Yves Gratton[3], Jean-Éric Tremblay[4], Bernard LeBlanc[1], Bert Klein[1], Michel Gosselin[5]

[1]GIROQ, Department of Biology, Laval University, Sainte-Foy, Québec G1K 7P4, Canada
[2]Laboratoire d'Océanographie de Villefranche (LOV), BP 28, 06234 Villefranche-sur-Mer Cedex, France
[3]INRS-Eau, 2800 rue Einstein, Sainte-Foy, Québec G1K 4C7, Canada
[4]McGill University, Department of Biology, 1205 Dr. Penfield, Montreal, Québec H3A 1B1, Canada
[5]Institut des sciences de la mer (ISMER), Université du Québec à Rimouski, 310 Allée des Ursulines, Rimouski, Québec G5L 3A1, Canada

[6]*Present address:* Institut des sciences de la mer (ISMER), Université du Québec à Rimouski, 310 Allée des Ursulines, Rimouski, Québec G5L 3A1, Canada

ABSTRACT: In order to understand the mechanisms responsible for the high productivity and biogeochemical cycling of carbon in the North Water Polynya (NOW), we determined physical properties and nutrient concentrations of the upper water column, and phytoplankton production, during spring/summer (April to July) 1998. Phytoplankton production of total organic carbon (P_{TOC}) was partitioned into production of dissolved and particulate organic carbon (P_{DOC} and P_{POC}, respectively), the latter being further partitioned into production of large and small phytoplankton (P_L and P_S, respectively) using 5 µm as threshold. The highest P_{TOC} was 6 g C m^{-2} d^{-1} at peak bloom. The fraction of P_{DOC} in P_{TOC} was lower in periods of high P_{TOC} than those of low P_{TOC}. Averaged over the whole polynya for the sampling period, P_{DOC} and P_{POC} accounted for 34 and 66% of the fixed carbon, respectively, and 81 and 19% of P_{POC} were in the P_L and P_S fractions, respectively. Variations in the integrated assimilation numbers of large and small phytoplankton were mostly explained by nutrients and irradiance. Even though P_{POC} was dominated by large phytoplankton, the sinking rates of the phytoplankton cells were relatively low (0 to 0.7 m d^{-1}), hence low export of P_{POC} to depth (17%), and relatively high potential transfer to large pelagic organisms through the herbivorous food web. This explains why the NOW is a major feeding and spawning area for fish, mammals and birds.

KEY WORDS: Primary production · Phytoplankton biomass · Dissolved organic carbon · Particulate organic carbon · P^B_{opt} · Export · Biogeochemical cycling · North Water (NOW) Polynya

INTRODUCTION

Polar oceans are particularly sensitive to global warming because increased temperature reduces ice concentration and increases water column stability. These 2 factors affect biological processes in marine ecosystems. Phytoplankton production plays a central role in the biogeochemical cycling of carbon in the upper ocean. For example, marine phytoplankton are fixing ca. 45 Gt yr^{-1} of organic carbon globally, of which about 1/3 is exported downwards (Falkowski et al. 1998). With global warming, the surface layer of the World Ocean is predicted to become more stratified by freshwater input from the melting of ice caps at high latitude, and increased temperature at lower latitudes. Over the long term, this would lead to reduced nutrient

*Email: zhi-ping.mei@uqar.qc.ca

supply from the depth to the surface, and hence, reduced production and export of organic carbon from the surface layer, thereby lowering the biologically driven flux of atmospheric CO_2 into the ocean (Falkowski et al. 1998).

In order to better estimate phytoplankton production of the World Ocean, more data on the characteristics of phytoplankton photosynthesis are needed (Sathyendranath et al. 1995). Chlorophyll-specific phytoplankton production, or assimilation number (P^B, g C g chl^{-1} h^{-1}) of marine phytoplankton, is required to estimate phytoplankton production from remotely sensed chlorophyll *a* concentrations. The up-scaling of *in vitro* phytoplankton production from single stations to large oceanic regions, and from instantaneous estimates to longer temporal scales, requires understanding the interactions between the characteristics of phytoplankton production and the physical and chemical properties of marine waters. This is because intermittent variations in the physical forcing frequently drive short-term and small-scale variations in phytoplankton production (Platt et al. 1989). In addition, the physical dynamics of the water column are believed to determine the partitioning of phytoplankton production and biomass among different size fractions (Tremblay et al. 1997b).

The role of the Arctic Ocean as a carbon source or sink is not certain as yet, due to insufficient knowledge of its primary production regime (Walsh 1989). Even though data on primary production in the Arctic Basin are accumulating (Kristiansen et al. 1994, Cota et al. 1996, Pomeroy 1997), especially since satellite images for chlorophyll have become available, data on the partitioning of production into different size fractions of biogeochemical significance, i.e. dissolved organic carbon (DOC) and particulate organic carbon (POC) of different sizes, started to become available only recently in the Arctic Basin (Gosselin et al. 1997) and Arctic polynyas (Pesant et al. 1996, Klein et al. 2002). Phytoplankton of different sizes differ in their physiological responses to physical and chemical conditions of the water column, following the laws of allometry (Chisholm 1992, Finkel & Irwin 2000). The flux of photosynthetically produced carbon by phytoplankton within the pelagic food web depends on the partitioning among DOC and POC of small and large phytoplankton (Legendre & Le Fèvre 1989, Tremblay & Legendre 1994, Legendre & Rassoulzadegan 1996). Field data and modeling exercises show that the production of large phytoplankton (P_L) often corresponds to new production (i.e. production supported by nitrate uptake), and that of small phytoplankton (P_S) to regenerated production (i.e. production supported by regenerated nitrogen, such as ammonium) (Tremblay et al. 1997a), although small phytoplankton can contribute substantially to nitrate uptake (Dauchez et al. 1996 for the Scotian Shelf and NW Atlantic, Bury et al. 2001 for the North Atlantic, Tremblay et al. 2000 for the Gulf of St. Lawrence). Therefore, not only the amount of inorganic carbon fixed by autotrophic photosynthesis, but its subsequent allocation to different size fractions are becoming focuses of production research.

The North Water Polynya (NOW, north of Baffin Bay between Ellesmere Island and Greenland) is one of the most productive areas in the Arctic (Stirling 1980, Klein et al. 2002, Tremblay et al. 2002b). The timing of photosynthetic fixation of organic carbon relative to such physical processes as the opening and closing of the ice cover and water column mixing determines the role of Arctic polynyas as carbon sinks or sources. In the present study, phytoplankton production in the NOW was partitioned into production of dissolved (P_{DOC}) and particulate organic carbon (P_{POC}), and the latter into large (P_L) and small sized fractions (P_S), using a threshold of 5 µm. The 5 µm threshold was selected based on the fact that mesozooplankton graze phytoplankton >5 µm most efficiently (Fortier et al. 1994). The purpose was to investigate the effects of physical and chemical characteristics, especially light and nutrients, on the photosynthetic characteristics of phytoplankton in different size classes, and to quantify the photosynthetic fixation of organic carbon into different size fractions. Our first hypothesis was that the photosynthetic characteristics of phytoplankton of different sizes varied differently with physical and chemical properties such as light, nutrients and water temperature, which would determine the production of carbon in different size fractions.

The NOW is known as a major spawning and feeding ground for marine mammals and birds (Stirling 1997), which suggests a strong link between the high phytoplankton biomass (Lewis et al. 1996, Mei et al. 2002), carbon production (Klein et al. 2002), silica and new production (Tremblay et al. 2002b) on the one hand, and the success of higher trophic levels on the other hand. Phytoplankton blooms produce large amounts of organic carbon, which is either exported to the pelagic food web or sinks out of the euphotic zone. The former leads to the production of renewable biological resources, and the latter may result in the sequestration of organic carbon at depth (Legendre 1990). Therefore, our second hypothesis was that a large fraction of the production in the NOW is transferred through the herbivorous food web rather than sinking out of the euphotic zone.

We tested these hypotheses during a multidisciplinary cruise on board the Canadian Coast Guard Ship (CCGS) 'Pierre Radisson' in the NOW, from April through July 1998. During the cruise, irradiance, nutrients, and size-fractionated phytoplankton biomass,

production and settling rates were determined, together with physical characteristics of the water column.

MATERIALS AND METHODS

Sampling. Sampling was conducted from 7 April through 20 July 1998 (Fig. 1). CTD (conductivity, temperature and depth) profiles, incident PAR (photosynthetically available radiation, 400 to 700 nm) on ship deck and over the euphotic zone (Mei et al. 2002), nutrients, including $NO_3^- + NO_2^-$ (hereafter referred to as N), PO_4^{3-} (hereafter referred to as P) and $Si(OH)_4$ (hereafter referred to as Si) (Tremblay et al. 2002a,b) and phytoplankton samples (Mei et al. 2002) were taken, along with ice cover observations (Mundy & Barber 2001). Surface incident irradiance (E_0) was continuously monitored on deck with a LI-COR LI-190 SA cosine corrected flat sensor. The euphotic-zone depth was defined as the depth of 1% surface irradiance. Samples for phytoplankton biomass (chlorophyll *a*, hereafter referred to as chl) and phytoplankton production were collected at depths corresponding to 100, 45, 30, 20, 10 and 1% of surface irradiance, at stations located on several transects (Fig. 1b).

Phytoplankton biomass (chl) and production. Water samples (500 to 1000 ml) were filtered on Whatman GF/F (0.7 µm pore size) and Nuclepore polycarbonate filters (5 µm pore size) to obtain total and large chl as a measure of phytoplankton biomass (B_T and B_L, respectively). Chl concentrated on filters was extracted with 90% acetone in cold (0 to 5°C) and dark conditions for 24 h. Chl in the extract was determined with a fluorometer (Turner Designs model 10) (Parsons et al. 1984). Biomass of small phytoplankton (B_S, <5 µm) was obtained by subtracting B_L from B_T.

For phytoplankton production determination, water samples (500 ml) from the euphotic zone were inoculated with 0.5 ml $NaH^{14}CO_3$ at 40 µCi ml^{-1} and incubated on deck for 24 h. The simulated *in situ* incubations started when the sun angle was the lowest of the day (Mingelbier et al. 1994). Irradiances in each incubator were adjusted with neutral density filters to approximate the irradiances at each sampling depth. During the incubation, surface water was continuously pumped through the incubators to maintain the incubation temperature close to that of the upper mixed layer, of which the depth (MLD) was established as that where the density increased by 0.01, or 0.04 from surface (Mei et al. 2002). Incubations were stopped by filtering the samples on Whatman GF/F filters (production of total phytoplankton, P_{POC} or P_T) or Nuclepore polycarbonate membrane filters (pore size: 5 µm; production of large phytoplankton, P_L). After filtration, the

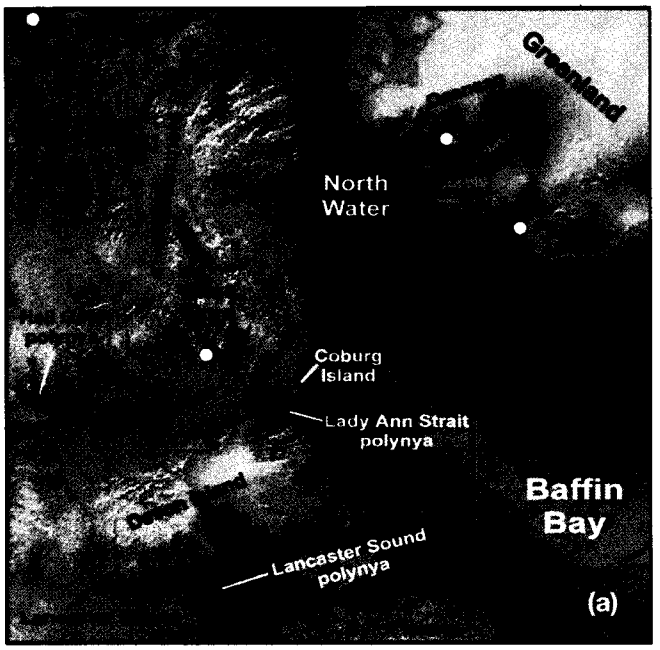

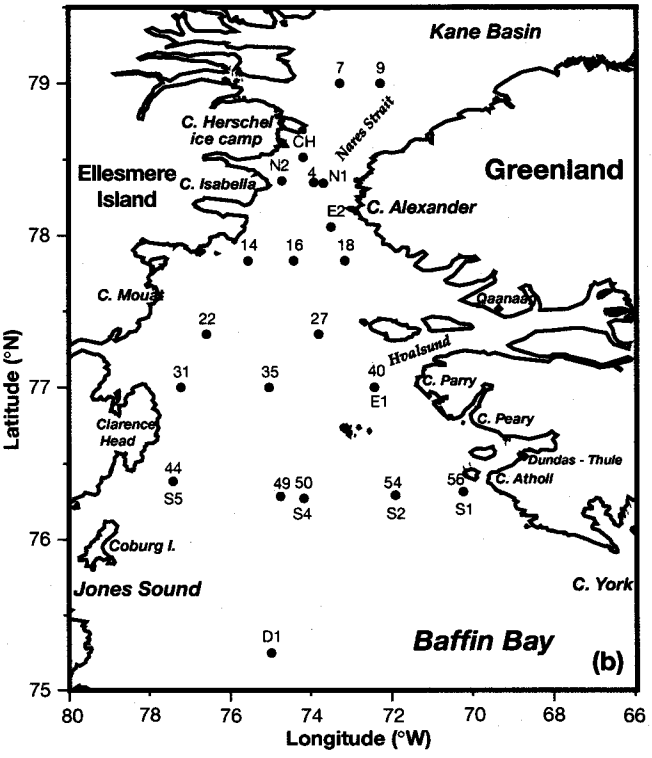

Fig. 1. (a) The satellite imagery of the North Water (NOW) polynya, taken on 10 May 1998 (courtesy of NOAA; image was processed by Dr. Martin Fortier). (b) Map of the NOW showing the locations of sampling stations. Stations marked with a number prefixed with a letter were mooring stations, sampled in July 1998. The other stations were sampled from April through June 1998

filters were dropped in liquid scintillation vials, and inorganic ^{14}C was removed by acidifying the filters with 0.2 ml 0.5 N HCl and continuously shaking the vials for at least 12 h in a fume hood. This was followed by addition of Ecolume scintillation cocktail (ICN).

A subsample (3 ml) of unfiltered incubated water was acidified with 0.5 ml 6 N HCl and shaken in the fume hood for at least 12 h, followed by addition of 0.5 ml 6 N NaOH to neutralize the sample and addition of 10 ml Ecolume. This provided the phytoplankton production of total organic carbon (P_{TOC}), i.e. the production of both particulate and dissolved organic carbon.

The samples with added Ecolume were kept in darkness and manually shaken several times during at least 48 h to ensure that all the radioactive materials on the filters were released into the Ecolume before scintillation counting. Samples were counted 2 to 3 times until counts were close in number. The measured radioactivity was transformed into production rates according to the JGOFS procedure (JGOFS 1996), using *in situ* total CO_2, provided by Dr. L. Miller (Institute of Ocean Sciences, Sidney, British Columbia, Canada). P_{DOC} was obtained by subtracting P_{POC} from P_{TOC}. The production of small phytoplankton (<5 µm, P_S) was obtained by subtracting P_L from P_T.

Areal phytoplankton production (mg C m^{-2} d^{-1}) and chl (mg m^{-2}) were obtained by trapezoidal integration of volumetric values of phytoplankton production (mg C m^{-3} d^{-1}) and chl (mg m^{-3}) from the depth profiles over the euphotic zone. Phytoplankton production was corrected for light attenuation due to ice cover, as detailed in Mei et al. (2002). The assimilation number of phytoplankton (P^B, g C g chl^{-1} h^{-1} or g C g chl^{-1} d^{-1}) was obtained by dividing phytoplankton production by chl.

The model of Platt et al. (1980) was used to describe the relationship between P^B (g C g chl^{-1} h^{-1}) and daily averaged irradiance (E_0, µmol photons m^{-2} s^{-1}) received by the samples during incubation, so as to obtain P^B_{opt} (the light-saturated P^B for a phytoplankton production profile, as defined by Behrenfeld & Falkowski 1997) when there was photoinhibition. Otherwise, the model of Jassby & Platt (1976) was fitted to the data. The model of Jassby & Platt (1976) was preferred when there was no photoinhibition because it has fewer parameters than the model of Platt et al. (1980) and therefore provided more stable estimates of parameters. Non-linear regressions were performed using the maximum likelihood procedure in Statistica (StatSoft).

Sinking rates (static) of phytoplankton cells taken from the depths of 50 and 1% surface irradiance were determined with settling columns (SETCOL) modified from Bienfang (1981), with a height of 54 cm, diameter of 9 cm and volume of 4.4 l. The SETCOLs were put in opaque sleeves (fixed with soft foam to isolate the SETCOLS from vibrations of the ship body) and set in a cold room (ca. 0°C) onboard the ship. Water samples were transferred to SETCOLs immediately after sampling and kept for ca. 6 h in darkness, following the procedure of Bienfang (1981).

Statistics. Model II linear regressions were computed with either the ordinary least square (OLS) procedure, for predictive purposes, or reduced major axis procedure (RMA), for estimating functional relationships (Legendre & Legendre 1998). In cases where the intercept was assumed to be 0 based on biological principles, the regression was forced through the origin. Path analyses were conducted to deconvolute the observed correlations among variables into direct and indirect causal relationships. Path coefficients were estimated by multiple ridge regressions after standardizing the raw data, and represented in path diagrams (Legendre & Legendre 1998).

RESULTS

Irradiance

The time course variation of daily averaged irradiance is shown in Fig. 2. In general, incident PAR increased from April, when the sampling began, to early June and into July, except for low values in mid to late June associated with foggy conditions.

Nutrients

Detailed descriptions of spatial and temporal distributions of nutrients are given in Tremblay et al. (2002a), and summarized in Table 1. Ratios of Si to N and of N to P are shown in Figs. 3 & 4, respectively. In April, Si:N ratios ranged from 1.0 to 1.8. In May, parallel to the phytoplankton bloom and the associated N consump-

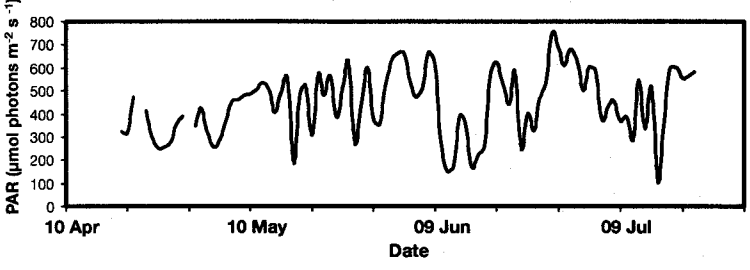

Fig. 2. Time series of PAR (photosynthetically available radiation) measured on deck, where samples for simulated *in situ* primary production were incubated

Table 1. Average values and ranges of physical and chemical variables, and assimilation numbers of total and large phytoplankton. E_0: surface incident irradiance; MLD: mixed-layer depth; N: $NO_3^- + NO_2^-$; P: PO_4^{3-}; Si: $Si(OH)_4$; P^{BT}: assimilation number of total phytoplankton; P^{BL}: assimilation number of large phytoplankton; P^{BT}_{opt}: light-saturated assimilation number of total phytoplankton; P^{BL}_{opt}: light-saturated assimilation number of large phytoplankton

Physical, chemical and production variables	Month			
	April	May	June	July
E_0 (µmol photons m^{-2} s^{-1})	94.9 (47–139)	321 (142–495)	304 (51–521)	300 (45–517)
MLD (m)	51 (20–114)	41 (13–54)	14 (5–25)	9 (5–17)
N (mmol m^{-3})	9.9 (7.9–10.7)	7.2 (0.3–10.2)	2.9 (<0.1–6.1)	3.2 (0.8–6.1)
P (mmol m^{-3})	1.3 (0.8–1.5)	1.21 (0.7–1.5)	0.8 (0.3–1.4)	0.78 (0.5–1.1)
Si (mmol m^{-3})	14.3 (7.6–17.4)	19.9 (4.8–23.0)	8.7 (1.0–24)	5.9 (2.6–11.4)
P^{BT} (g C g chl^{-1} h^{-1})	15.7 (2.5–44.7)	11.3 (6.7–24.2)	10.5 (1.5–27.5)	5.7 (1.4–10.0)
P^{BL} (g C g chl^{-1} h^{-1})	17.3 (3.6–40.8)	11.8 (6.6–14.7)	9.0 (1.2–21.8)	4.7 (1.3–8.6)
P^{BT}_{opt} (g C g chl^{-1} h^{-1})	2.1 (0.8–4.3)	1.3 (0.9–1.6)	1.0 (0.8–1.7)	0.8 (0.3–1.0)
P^{BL}_{opt} (g C g chl^{-1} h^{-1})	3.2 (1.3–5.7)	1.3 (0.8–2.0)	0.8 (0.4–1.9)	0.7 (0.3–1.2)

tion, the Si:N ratio increased to 1.4–4.4 at most stations. The ratio reached a remarkable value of 14.3 at Stn 54, southeast of the polynya, where the peak phytoplankton bloom was taking place. In June, Si:N ranged from 2.0 to 11.4, with high values observed at stations with a sustained phytoplankton bloom, and low values in the southeast of the polynya, where the phytoplankton bloom declined. In July, the ratio was close to that of April, except for a high value of 4.2 at Stn N1 in northern Smith Sound, which is the outlet of the Arctic flow. At all stations and times, Si:N was >1.0.

The N:P ratios were rather uniformly distributed over the polynya in April, ranging from 5.5 to 8.6, except for the highest value of 10 at Stn 40. In May, the ratio ranged from 5.1 to 6.9, except for the extremely low value of 0.8 at Stn 54 associated with the peak phytoplankton bloom and N depletion. In June, the ratio decreased at stations on the Greenland side of the polynya, and south of 77° N (0.5 to 3). Higher values of 3 to 8 were observed at stations north of 77° N, and on the Canadian side of the polynya. In July, the ratios were rather uniformly distributed (3 to 5) over the polynya, the highest value of 15 being observed at Stn D68 in northern Baffin Bay. The N:P ratio was always <15, indicating that P was not the limiting element, by reference to the Redfield ratio of 16:1 (Redfield et al. 1963).

The observed variations in Si:N and N:P were mainly associated with N drawdown following the development of phytoplankton bloom. It appears that N was the most likely limiting nutrient in the NOW, by reference to the Redfield ratio (Redfield et al. 1963). Therefore, only N is included in the path analyses below.

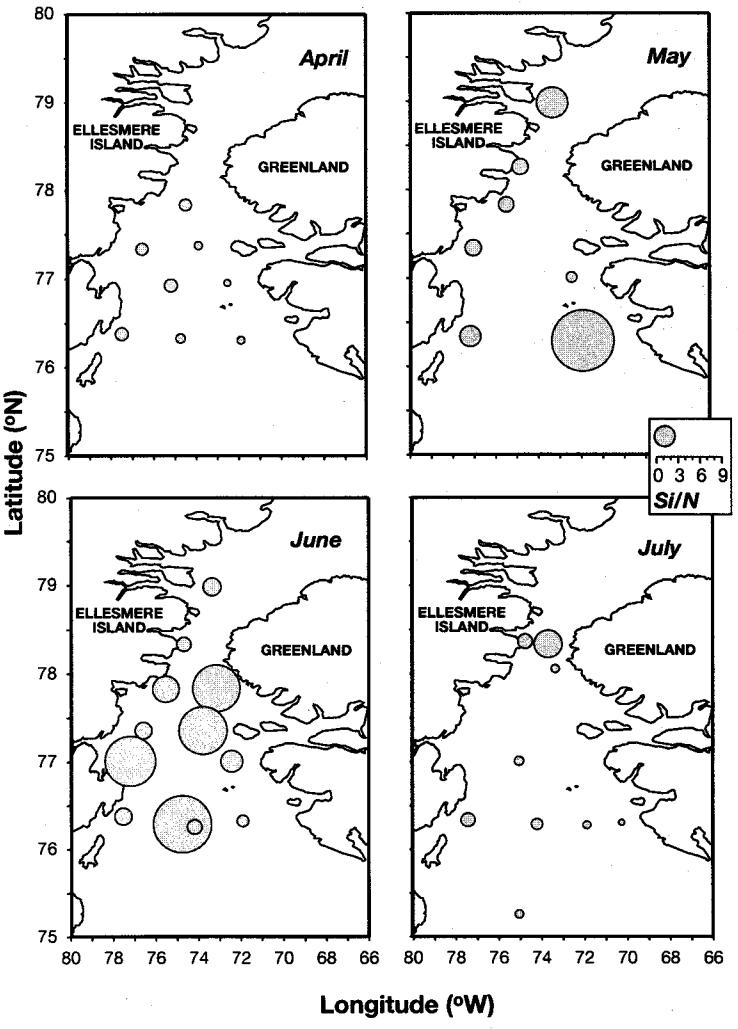

Fig. 3. Depth-integrated average concentration ratios (mol:mol) of Si ($Si(OH)_4$) to N ($NO_3^- + NO_2^-$) in the euphotic zone from April to July 1998

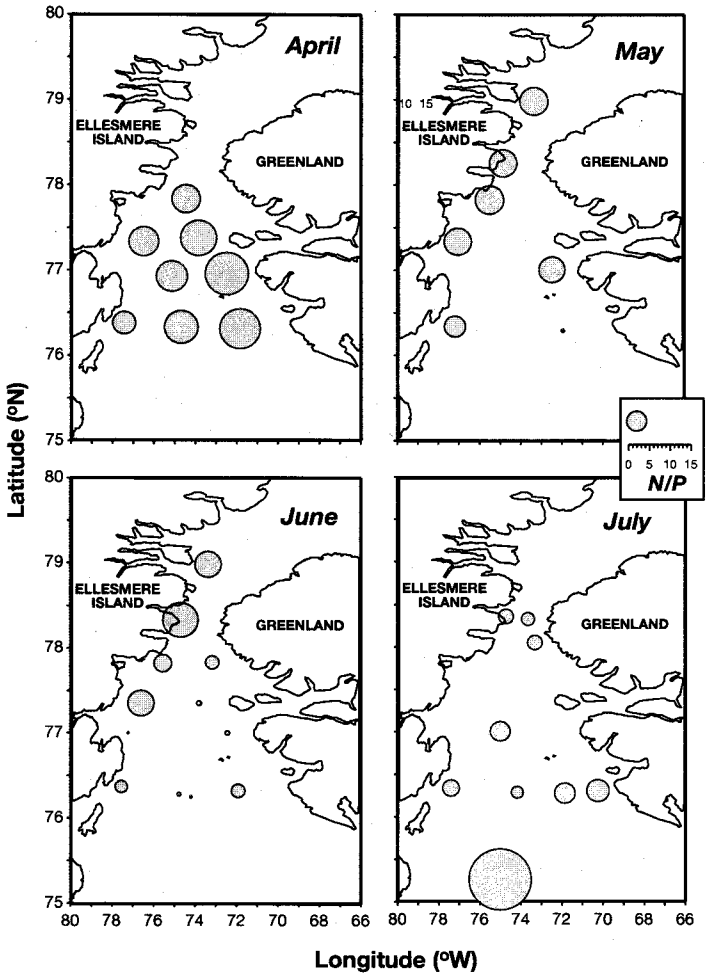

Fig. 4. Depth-integrated average concentration ratios of N ($NO_3^- + NO_2^-$) to P (PO_4^{3-}) in the euphotic zone from April to July 1998

Phytoplankton production

Fig. 5 shows the spatial patterns of phytoplankton production during April through July. In April, high P_{TOC} (0.4 to 1 g C m^{-2} d^{-1}) was observed at stations on the Greenland side (e.g. Stns 27, 40 and 54), and very low values (<0.2 g C m^{-2} d^{-1}) were observed on the Canadian side (Stns 22 and 44, Fig. 5a). In May, the highest P_{TOC} occurred on the Greenland side, where the bloom reached its peak (Fig. 5b). The highest value (6.0 g C m^{-2} d^{-1}) was observed at Stn 40, followed by 4.8 g C m^{-2} d^{-1} at Stn 54 on the Greenland side. Values for northern stations (e.g. Stns 2, 7 and 14) were low (<0.2 g C m^{-2} d^{-1}). Because of a strong storm, there are no data for Stns 18, 22 and 27. P_{TOC} increased from May to June at the northern stations, and southern stations on the Canadian side (Fig. 5b,c). However, P_{TOC} decreased by ~50% at stations southeast of the polynya (e.g. Stn 40) on the Greenland side from May to June. Further south, phytoplankton production decreased by nearly 100% from May to June. In July, P_{TOC} at stations in the northern part of the polynya also decreased, and P_{TOC} over the polynya was low (<0.1 to 2.4 g C m^{-2} d^{-1}, Fig. 5d). Therefore, the phytoplankton bloom ended in late June in the south, and in early July in the North of the polynya.

The relationships between P_{TOC}, E_0, N, and water temperature are illustrated in Fig. 6. P_{TOC} >2 g C m^{-2} d^{-1} are associated with high E_0. Some of these high P_{TOC} also appear to be associated with low N, which is, in turn, associated with higher water temperature given the inverse relationship (Spearman $r_s = -0.85$, $n = 33$, $p < 0.01$) between N and water temperature (Fig. 6b). On the contrary, most P_{TOC} <2 g C m^{-2} d^{-1} are associated with either E_0 <300 µmol photons m^{-2} s^{-1}, or high N, but low water temperature (Fig. 6a,b).

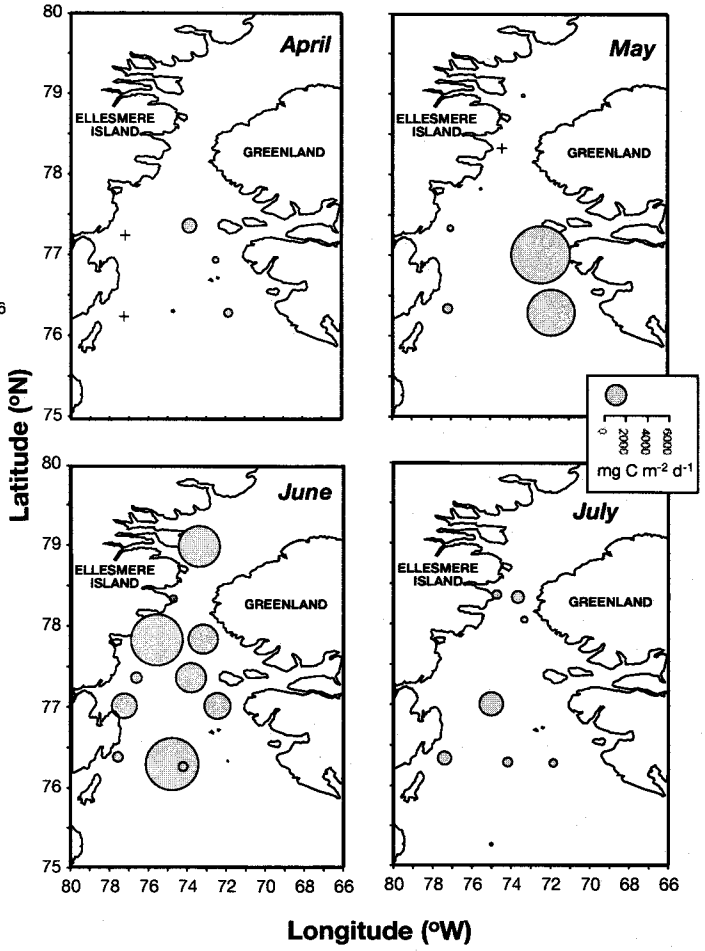

Fig. 5. Horizontal distribution of P_{TOC} (production of total organic carbon) from April through July. The value of P_{TOC} is linearly proportional to the diameter of the bubbles. '+' indicates the positions of stations with total phytoplankton production values <0.2 g C m^{-2} d^{-1}

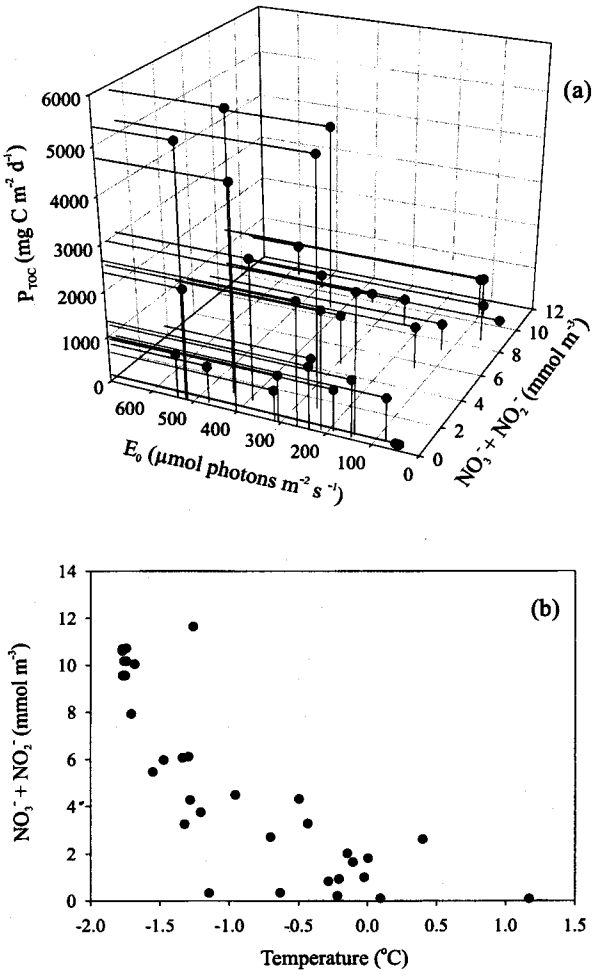

Fig. 6. (a) 3D plot of P_{TOC} against E_0 (surface irradiance) and N ($NO_3^- + NO_2^-$), and (b) scatter plot of the inverse relationship (Spearman $r_s = -0.85$, $n = 33$, $p < 0.01$) between N and water temperature

Production and biomass of phytoplankton in different size fractions

Relationship between phytoplankton production and chl

Areal chl integrated over the euphotic zone (mg m^{-2}) explained a large fraction of the variance of P_{TOC}, P_{POC} and P_{DOC} (Fig. 7). The respective regression (OLS) equations through the origin are listed in Table 2 (Eqs. 4 to 6). The highest slope among Eqs. (4) to (6) is for P_{TOC} on chl. Judging from the coefficients of determination, chl accounted for higher variability of P_{TOC} than of P_{POC} or P_{DOC} separately. Similarly, phytoplankton production of large phytoplankton was largely explained by the corresponding biomass (Eq. 7 in Table 2).

Percent P_{TOC} as P_{POC} and P_{DOC}

P_{POC} was significantly related to P_{TOC} (Fig. 8). The slopes (±95% CI) of the regressions (OLS) of P_{POC} on P_{TOC} are 0.9 (±0.23) and 0.5 (±0.21) for high P_{TOC} (>2 g C m^{-2} d^{-1}) and low P_{TOC} (<2 g C m^{-2} d^{-1}), respectively (Eqs. 1 & 2 in Table 2), however, the difference is not significant at $\alpha = 0.05$. A regression (OLS) through the origin was computed for the whole data set, resulting in an overall slope of 0.66 (Eq. 3 in Table 2).

The slope of the regression of P_L on P_T (Eq. 8 in Table 2) indicates that, on average, the production of large phytoplankton accounted for 81% of total

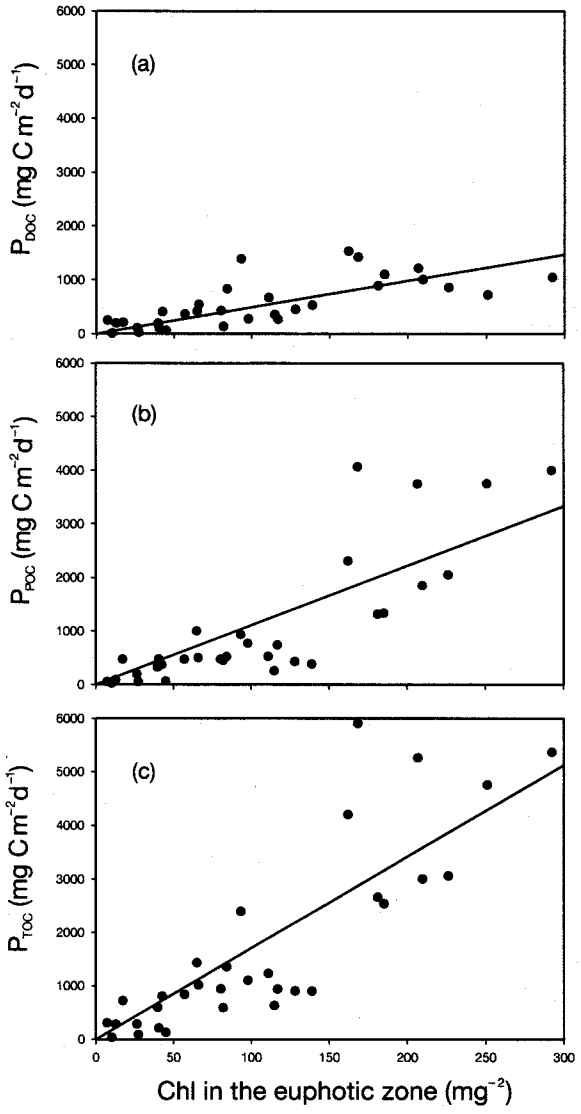

Fig. 7. Scatterplots and regressions of (a) P_{DOC}, (b) P_{POC} and (c) P_{TOC} on chl through the origin. Regression equations are given in Table 2

phytoplankton production; however, the slope of the regression of B_L on B_T (Eq. 9, Table 2) indicates that the biomass of large phytoplankton accounted for 85% of total phytoplankton biomass, when integrated for the whole polynya during spring–summer.

Relationships between P_L and P_S, and B_L and B_S

The biomass of small phytoplankton increased linearly with that of large phytoplankton when B_L was <160 mg chl m^{-2} (Fig. 9a; Eq. 10 in Table 2). Above B_L = 160 mg chl m^{-2}, B_S progressively decreased to undetectable levels as B_L approached 300 mg m^{-2} (Fig. 9a). Corresponding production of small phytoplankton increased linearly with that of large phytoplankton (Fig. 9b, Eq. 11 in Table 2). The 2 slopes are significantly lower than 1, meaning that the biomass and production of small phytoplankton, and consequently their rate of biomass increase, were significantly lower than those of large phytoplankton.

Table 2. Summary of the relationships among phytoplankton production, biomass and sinking rates in different size fractions. Eqs. (10) & (11): Model II regressions (reduced major axis [RMA] procedure); other equations: ordinary least square regressions. r^2: coefficient of determination; p: probability slope = 0. 95% confidence intervals of regression slopes are given as (±95% CI). P_{POC}: production of particulate organic carbon; P_{TOC}: production of total organic carbon; P_{DOC}: production of dissolved organic carbon; P_L: production of large phytoplankton; B_L: biomass of large phytoplankton; B_S: biomass of small phytoplankton; P_S: production of small phytoplankton; F_T: sinking flux of total phytoplankton; F_L: sinking flux of large phytoplankton

Equations	Eq.		n	p
P_{POC} = 0.9 (±0.23) P_{TOC} – 992.3[a]	1	r^2 = 0.95	10	<0.05
P_{POC} = 0.5 (±0.21) P_{TOC} + 38.6[b]	2	r^2 = 0.7	22	<0.01
P_{POC} = 0.66 (±0.04) P_{TOC}	3	r^2 = 0.96	32	<0.01
P_{TOC} = 17.1 (±4.7) chl	4	r^2 = 0.71	31	<0.01
P_{POC} = 11.1 (±1.83) chl	5	r^2 = 0.66	33	<0.01
P_{DOC} = 4.9 (±0.82) chl	6	r^2 = 0.51	32	<0.01
P_L = 10.6 (±0.1.8) B_L	7	r^2 = 0.81	35	<0.01
P_L = 0.81 (±0.04) P_T	8	r^2 = 0.98	34	<0.01
B_L = 0.85 (±0.04) B_T	9	r^2 = 0.98	36	<0.01
B_S = 0.38 (±0.07)B_L + 2.9[c]	10	r^2 = 0.79	29	<0.001
P_S = 0.43 (±0.05) P_L + 22.2[c]	11	r^2 = 0.90	30	<0.001
F_T = 0.015 (±0.002) B_T	12	r^2 = 0.90	32	<0.01
F_L = 0.018 (±0.002) B_L	13	r^2 = 0.91	25	<0.05

[a]P_{TOC} > 2 g C m^{-2} d^{-1}
[b]P_{TOC} < 2 g C m^{-2} d^{-1}
[c]Model II regression (RMA procedure)

Light-saturated (P^B_{opt}) and depth-integrated rates (P^B) of particulate phytoplankton production in different size fractions

Path analyses (Fig. 10) were used to identify direct and indirect causal effects of E_0, MLD, N and P^B_{opt} on P^B integrated over the euphotic zone. Comparing the path diagrams for P^{BT} and P^{BL} shows that P^{BT} and P^{BL} responded differently to the independent variables (Fig. 10). The path coefficient from E_0 to P^{BT} is significant (Fig. 10a), but not that from E_0 to P^{BL} (Fig. 10b). The path coefficient from N to P^{BT} is significant, but not for that from N to P^{BL}. However, N indirectly affects P^{BL} and P^{BT} similarly, i.e. through P^{BL}_{opt} and P^{BT}_{opt}, respectively.

Sinking rates of phytoplankton

The sinking rates of phytoplankton (S) ranged from 0.1 to 0.7 m d^{-1}, between April and July. The variations in sinking rates were small compared to those in phytoplankton biomass (Fig. 11).

The daily sinking fluxes of chl out of the euphotic zone (F, mg chl m^{-2} d^{-1}) were estimated by multiplying the mean concentration of chl integrated over the euphotic zone (B_V, mg m^{-3}) by S (m d^{-1}). The mean sinking flux of total chl (F_T) was 0.35 (range: 0.01 to

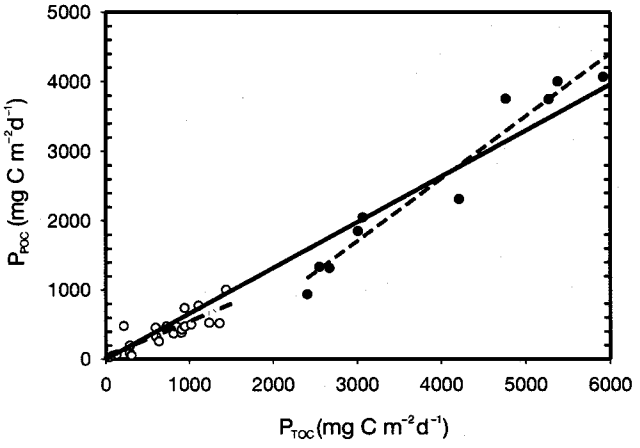

Fig. 8. Scatter plots and regressions of P_{POC} on P_{TOC}. The data were separated in 2 groups, P_{TOC} > 2 g C m^{-2} d^{-1} (●, Eq. 1) and P_{TOC} < 2 g C m^{-2} d^{-1} (○; Eq. 2). Solid line: overall regression through the origin; Eq. 3

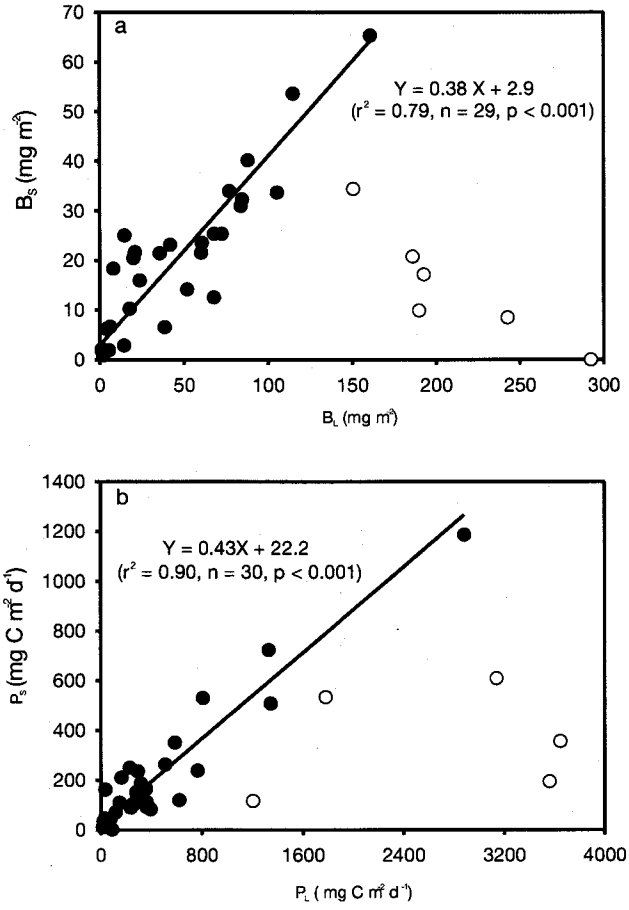

Fig. 9. Relationships between (a) the chl of small (B_S) and large phytoplankton (B_L), where the B_S starts to decrease when the B_L >160 mg chl m^{-2} (clear circles), and (b) between production of small (P_S) and large phytoplankton (P_L). Clear circles were not included in Model II (reduced major axis [RMA] procedure) regression analyses

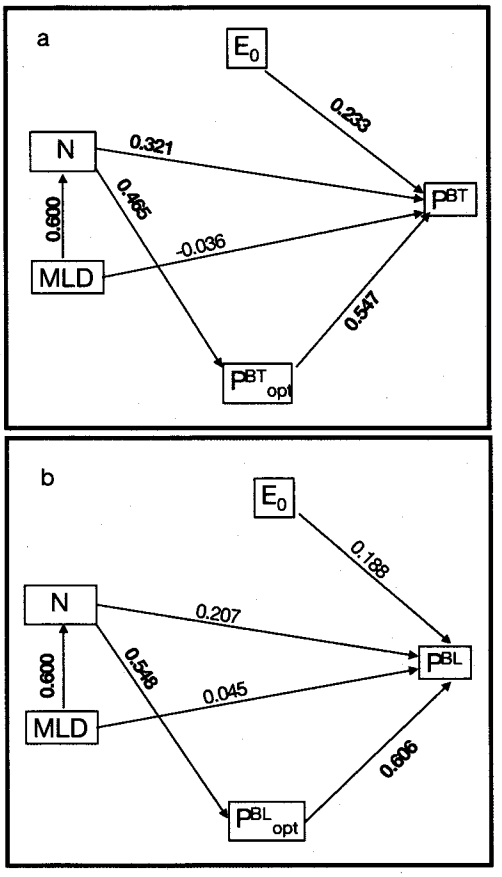

Fig. 10. Path analyses of P^B of (a) total (P^{BT}) and (b) large phytoplankton (P^{BL}) with respect to N (NO_3^- + NO_2^-), E_0, MLD (mixed layer depth) and P^B_{opt} of total (P^{BT}_{opt}) or large phytoplankton (P^{BL}_{opt}), respectively. The arrows indicate the direction of the effect of one variable on another. The values associated to the arrows are the standardized path coefficients. Bold-type path coefficients are significant at $p < 0.05$

0.85), 1.38 (range: 0.02 to 5.0), 2.71 (range: 1 to 6) and 0.67 (range: 0.1 to 1.5) mg chl m^{-2} d^{-1}, in April, May, June and July, respectively. The sinking flux for large phytoplankton (F_L) was 1.4 (0.2 to 5.2), 2.8 (1.1 to 6.8) and 0.6 (0.01 to 1.2) mg chl m^{-2} d^{-1}, in May, June and July, respectively. Data for sinking rates of large phytoplankton are not available for April.

F_T and F_L were regressed (OLS) through the origin on the corresponding areal chl integrated over the euphotic zone (B_T and B_L, mg m^{-2}, respectively) (Eqs. 12 & 13 in Table 2). The slopes of the regressions show that 1.5 and 1.8% of the standing chl stocks of total and large phytoplankton in the euphotic zone, respectively, sank below the euphotic zone daily.

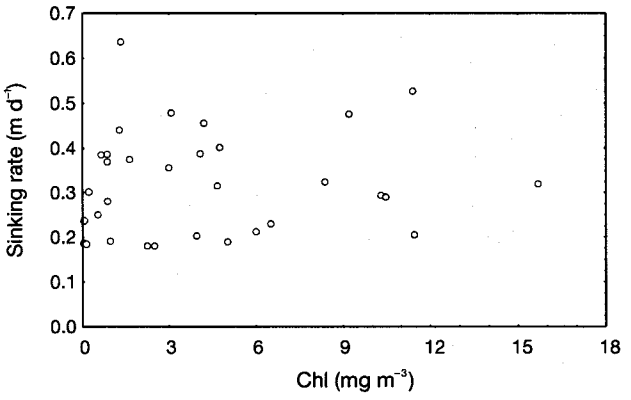

Fig. 11. Scatterplot of phytoplankton sinking rates (m d^{-1}) versus mean integrated chl in the euphotic zone (mg m^{-3})

DISCUSSION

Differential responses of P^B of large and small phytoplankton to physical and chemical properties in the water

Behrenfeld & Falkowski (1997) found that depth-integrated P^B is largely determined by light-saturated P^B, P^B_{opt}, over the World Ocean. P^B_{opt} in the present study was obtained from 24 h incubation, and therefore represents the photosynthetic characteristics of phytoplankton adapted to growth irradiance. This is different from the corresponding parameter of the photosynthesis versus irradiance relationship (Platt et al. 1980) obtained under short-term incubation (<4 h), which represents the photosynthetic characteristics of phytoplankton incubated under a different irradiance to that in their growth environment (Sakshaug et al. 1989, Cullen 1990).

In the present study, path analysis showed that N regulates P^B indirectly through its positive effect on P^B_{opt} for both total and large phytoplankton (Fig. 10). This seems to be different from what was observed at the Bermuda Atlantic Time Series station (BATS, 32° 15′ N, 65° 45′ E), where Johnson & Howd (2000) found a negative correlation between P^B_{opt} and nitrate concentration. They invoked several reasons to explain this, including multiple nutrient limitation, high nitrogen recycling and micronutrient limitation. However, high nitrate concentration in their data series covaried with the input of deep, cold water due to deepened mixed layer, which may imply a negative effect of temperature on P^B_{opt} that would weaken the correlation between nitrate and P^B_{opt}.

The above mentioned dependence of P^B_{opt} on nutrients in the NOW agrees with similar observations in the equatorial Pacific. The increased photosynthetic capacity caused by increased nutrient supply led to an almost 3-times increase in daily phytoplankton production there (Barber et al. 1996). Nutrient supply affects the quantum yield of photosynthesis (Sathyendranath et al. 1999), and the optical characteristics and subsequent carbon fixation of phytoplankton (Berman-Frank & Dubinsky 1999, and references therein). The studies cited above concern short-term incubations (4 to 6 h), but similar mechanisms apply to long incubations (Cullen et al. 1990). Therefore, in the NOW, and probably most marine waters, the nutrient supply controls P^B_{opt}, and thereby P^B integrated over the euphotic zone, by regulating the photosynthetic performance of phytoplankton, as observed in the western North Atlantic (Platt 1992).

Differences in the responses of P^{BL} and P^{BS} (P^B of small phytoplankton) to E_0 and N can be inferred from the different responses of P^{BT} and P^{BL} to E_0 and N. As total phytoplankton includes both large and small phytoplankton, although dominated by large phytoplankton in the NOW, the significant causal effect from N to P^{BT} and non-significant causal effect from N to P^{BL} suggest that the N had significant causal effects on P^{BS}. For the similar reason, the lower causal effects of N on P^{BT}_{opt} (P^B_{opt} of total phytoplankton), and of P^{BT}_{opt} on P^{BT} than those of N on P^{BL}_{opt}, and of P^{BL}_{opt} on P^{BL} suggest that the causal effects from N to P^{BS}_{opt} (P^B_{opt} of small phytoplankton), and of P^{BS}_{opt} on P^{BS} were not significant. N limited P^{BL} indirectly by limiting their maximum photosynthetic capacity in the upper euphotic zone, which was not the case for small phytoplankton. Hence, P^{BL}_{opt} was more N-dependent than P^{BS}_{opt}.

Similarly, the significant effect of E_0 on P^{BT} (Fig. 10a) can be attributed to a light dependence of small phytoplankton, because the path coefficient from E_0 to P^{BL} (Fig. 10b) is not significant. This suggests that during the course of the phytoplankton bloom, the increased biomass of large phytoplankton took out the irradiance niche of small phytoplankton in the euphotic zone, which gave a competitive advantage to large phytoplankton. This conjecture is supported by the fact that the biomass and production of small phytoplankton decreased as large phytoplankton reached >150 mg chl m^{-2} (Fig. 9). This was not likely caused by N depletion, because the latter did not occur until P_L and B_L reached their highest levels. In addition, small phytoplankton should be more competitive than large phytoplankton at taking up nutrients under low nutrient concentrations, given their higher surface to volume ratios. The <1 slopes of the regressions of B_S on B_L and P_S on P_L suggest that large phytoplankton had higher growth rates than their smaller counterparts. Therefore, we think that the development of large phytoplankton caused shading of small phytoplankton. Large phytoplankton exhibit higher quantum yield than small phytoplankton when nutrients are replete (Sathyendranath et al. 1999), which could explain why large phytoplankton were less light-dependent than small phytoplankton in the NOW. Figueiras et al. (1999) also observed a lack of light limitation when the phytoplankton community was dominated by large diatoms and *Phaeocystis* in the Weddell Sea in summer.

The potential effects of water temperature on P^B should be important. However, we were not able to continuously monitor water temperature during incubation, and the number of variables that could be included in path analyses is limited. Therefore, we did not try to investigate the effects of water temperature on P^B in path analyses. Direct assessment of the responses of P^B of small phytoplankton is difficult, because the biomass and production of small phytoplankton were obtained by differences between those of total and large phytoplankton. The resulting values

of production and biomass of small phytoplankton are very small, resulting in larger errors.

However, the above conclusions are consistent with our first hypothesis that the photosynthetic characteristics of large phytoplankton respond to physical and chemical properties of the water column differently than those of small phytoplankton. Therefore, different physical and chemical properties will ultimately lead to variations in phytoplankton production in different size fractions.

Partitioning of P_{TOC} into different size fractions (P_{DOC}, P_L, and P_S): biogeochemical significance

The partitioning of carbon fixed into P_{DOC} and P_{POC}, depending on P_{TOC} level (Fig. 8), agrees with the cross-system comparisons of Carlson et al. (1998), who found that in the eutrophic Ross Sea, 89% of the C fixed by phytoplankton was incorporated into POC and 11% into DOC, whereas in the oligotrophic Sargasso Sea, 86% of the inorganic C fixed was incorporated into DOC and 14% into POC. In the NOW, low production values were observed at stations with either one of the following unfavourable growth conditions: low irradiance, low temperature (<–1°C), or low N (Fig. 6).

Baines & Pace (1991) and Obernosterer & Herndl (1995) observed that phytoplankton DOC exudation increased with increasing N:P in the inorganic nutrients, as a response to P limitation. That led Karl et al. (2001) to hypothesize that the increased percentage of P_{DOC} in the subtropical North Pacific Gyre resulted from a shift of the system from nitrogen to phosphorus limitation. However, N:P in the NOW was lower than the Redfield ratio, showing no evidence of P limitation (Fig. 4). On the contrary, N depletion was observed at stations southeast of the polynya by the end of June (Figs. 3 & 4). In fact Obernosterer & Herndl (1995) also observed increased extracellular DOC exudation at an N:P ratio of <16. Thus, high DOC production does not seem to be specifically associated with P limitation.

Overall, P_{DOC} in the NOW made up a remarkably high fraction (34%) of P_{TOC}, and thus provided large amounts of substrate for the microbial food web. Karl et al. (1998) indicated that omission of P_{DOC} could result in a significant underestimation of global phytoplankton production, based on recent estimates of P_{DOC} and P_{POC} in the subtropical North Pacific Ocean. The higher slope of the regression of chl on P_{TOC} than that on P_{POC} alone, and the fact that chl accounted for higher variability of P_{TOC} than of P_{POC} alone (Eqs. 4 & 5 in Table 2), not only suggest that P_{DOC} is a significant fraction of P_{TOC}, but also supports the argument of Baines & Pace (1991) that DOC production is constrained by the total C fixed, instead of passive diffusion from phytoplankton cells.

There are few comparable data of P_{DOC} for Arctic waters (Wheeler et al. 1996, Gosselin et al. 1997, Vernet et al. 1998). The value of percent P_{DOC} in the present study (34%, derived from the slope of Eq. 3 in Table 2) agrees with those reported for the central Arctic Ocean (Wheeler et al. 1996, Gosselin et al. 1997), where P_{DOC} was <40% of P_{TOC} at most stations, and as high as ca. 70% at a few stations between 75 and 85°N. However, the highest observed P_{DOC} there (0.38 g C m^{-2} d^{-1}) is much lower than the highest in the NOW (>1.0 g C m^{-2} d^{-1}).

In polar regions, 24 h daylight provides sufficient sea surface irradiance to enhance the photosynthetic fixation of carbon, while the loss of the carbon due to respiration in the night is much less than that at lower latitudes. Extremely high irradiance may increase the percent P_{DOC}, especially when the CO_2:O_2 ratio is reduced because of continuous photosynthesis (Zlotnik & Dubinsky 1989, Wood & Van Valen 1990). Phytoplankton in nutrient-depleted waters may stop protein synthesis and growth, while the continuing photosynthetic carbon fixation favours DOC exudation (de Madariaga & Fernandez 1990, Søndergaard et al. 2000).

DOC production in the NOW is remarkably high (0.58 g C m^{-2} d^{-1}), and the absolute values of P_{DOC} may be among the highest reported in any ocean. This is largely because of the high P_{TOC}. The contribution of DOC to deep export, via convective mixing in winter, depends on the temporal scale of its remineralization, which is not presently known in the NOW, nor the biodegradability of the produced DOC. The respiration of organic carbon back to CO_2 within the microbial food web is highly dependent on temperature, generally more than phytoplankton production in polar waters (Pomeroy & Deibel 1986, Yager & Deming 1999, Rivkin & Legendre 2001). Therefore, the high DOC production, which is associated with high P_{TOC} in the NOW, could result in a significant reduction of CO_2 in the euphotic zone during the spring/summer season. As much as 250 µmol kg^{-1} of total dissolved inorganic carbon (DIC) reduction in the upper water column in the NOW was observed by the end of the spring–summer phytoplankton bloom (Miller et al. 2002).

P_{POC} in the present study (ca. 5 g C m^{-2} d^{-1}) is among the highest values reported for polar seas. On the shelf and in the marginal ice zone of the Weddell Sea, Southern Ocean, the highest reported values are 2.6 g C m^{-2} d^{-1} (Park et al. 1999). In the West Greenland Sea, a value of 3.2 g C m^{-2} d^{-1} was reported for the summer 1993 (Jensen et al. 1999). Both production and biomass of P_{POC} are dominated by large phytoplankton, as shown in Eqs. (8) & (9) (Table 2). Therefore, most of the P_{POC} could be potentially exported to herbivorous food web, or towards depth.